Taylor & Francis
Taylor & Francis Group

AEROSOL SCIENCE AND TECHNOLOGY

Water vapor depletion in the DMT Continuous Flow CCN Chamber: effects on supersaturation and droplet growth.

Journal:	*Aerosol Science & Technology*
Manuscript ID:	AST-MS-2010-183.R1
Manuscript Type:	Original Manuscript
Date Submitted by the Author:	n/a
Complete List of Authors:	Lathem, Terry; Georgia Inst of Technology, School of Earth and Atmos Sciences Nenes, Athanasios; Georgia Inst of Technology, School of Earth and Atmos Sciences
Keywords:	aerosol-cloud interactions, cloud condensation nuclei (CCN), measurement

Water vapor depletion in the DMT Continuous Flow CCN Chamber: effects on supersaturation and droplet growth.

Terry L. Lathem

School of Earth & Atmospheric Sciences, Georgia Institute of Technology, Atlanta, GA 30332 (terry.lathem@eas.gatech.edu)

Athanasios Nenes*

Schools of Earth & Atmospheric Sciences and Chemical & Biomolecular Engineering, Georgia Institute of Technology, Atlanta, GA 30332 (athanasios.nenes@gatech.edu)

Short title: SUPERSATURATION DEPLETION IN THE CFSTGC

*corresponding author

Abstract

The Continuous-Flow Streamwise Thermal-Gradient Cloud Condensation Nuclei Counter (CFSTGC) is a commercially-available instrument that is widely used for laboratory and field measurements of cloud condensation nuclei (CCN). All studies to date assume that the supersaturation profile generated in its growth chamber is not influenced by the condensation of water vapor upon the growing CCN. The validity of this assumption, however, has never been systematically explored. This work examines when water vapor depletion from CCN can have an important impact on supersaturation, measured CCN concentration and droplet growth. A fully coupled numerical flow model of the instrument is used to simulate the water vapor supersaturation, temperature, velocity profiles and CCN growth in the CFSTGC for a wide range of operation and CCN concentrations. Laboratory CCN activation experiments of polydisperse calibration aerosol (with a DMT CFSTGC operated in constant flow mode) are used to evaluate the simulations. The simulations and laboratory experiments are then generalized using a scaling analysis of the conditions that lead to supersaturation depletion. We find that CCN concentrations below 5000 cm^{-3} (regardless of their activation kinetics or instrument operating conditions) do not decrease supersaturation and outlet droplet diameter by more than 10%. For larger CCN concentrations, a simple correction can be applied that addresses both the depression in supersaturation and droplet size.

1. Introduction

The Continuous-Flow Streamwise Thermal Gradient Cloud Condensation Nuclei (CCN) Chamber [CFSTGC; Roberts and Nenes, 2005] and its commercialization by Droplet Measurement Technologies [Lance et al., 2006; Rose et al., 2008] has enabled large strides in understanding and parameterizing the CCN activity of atmospheric aerosol. This is in large part due to the flexibility and fast time response of the instrument, which allows its use in a number of configurations to complement aerosol and cloud studies. Used as a "counter" in constant flow mode [e.g., Roberts and Nenes, 2005; Lance et al., 2006; Rose et al., 2008] or as a "spectrometer" in scanning flow mode [Moore et al., 2009], it provides the total concentration of CCN as a function of supersaturation. When coupled with a differential mobility analyzer (DMA) operated in voltage-stepping [e.g., Lance, 2007; Petters et al., 2009; Rose et al., 2010] or voltage-scanning mode [Moore et al., 2010], size-resolved CCN measurements enables the parameterization of composition impacts on cloud droplet formation [Rose et al., 2010; Petters et al., 2009; Petters and Kreidenweis, 2007; Wex et al., 2007; Padró et al., 2007; Lance, 2007; Asa-Awuku et al., 2010], the characterization of chemical ageing and mixing state of aerosol [Roberts et al, 2010; Cubison et al., 2008; Kuwata et al., 2008; Lance, 2007], and provide insight on the molar volume and surfactant characteristics of the water-soluble carbonaceous aerosol fraction [e.g., Padró et al., 2007; Engelhart et al., 2008; Asa-Awuku et al., 2009, 2010].

The CFSTGC has also been used to study the activation kinetics of ambient CCN, using the final activated CCN drop size at the end of the growth column as the metric of CCN growth rate. One approach, Threshold Droplet Growth Analysis [TDGA; Engelhart et al., 2008; Sorooshian et al., 2008; Bougiatioti et al., 2009; Asa-Awuku et al., 2009; Lance et

al., 2009, Murphy et al., 2009] uses a "reference" critical supersaturation - droplet size curve to define the minimum size of droplets that are produced from rapidly-activating CCN (such as $(NH_4)_2SO_4$ and NaCl). If ambient CCN produce droplets that lie below the reference curve (i.e., produce smaller droplets than the reference at a given supersaturation), the ambient CCN are then said to exhibit slower activation kinetics than the reference. If kinetic delays are detected, then knowledge of the aerosol size distribution and hygroscopicity can then be combined with a numerical model of the instrument to parameterize the slow activation kinetics in terms of a water-vapor uptake coefficient [e.g., Asa-Awuku et al., 2009] or a dissolution timescale [e.g., Chuang et al., 2006]. When size-resolved CCN measurements are carried out, the observed droplet distribution at the exit of the chamber can be inverted (using an instrument model) to provide distributions of kinetic parameters [Ruehl et al., 2008, 2009] which provides particularly powerful insight on the kinetic heterogeneity of atmospheric CCN.

A basic assumption in all studies using the CFSTGC is that the water vapor field in the growth chamber is not affected by the condensation of water onto the growing CCN. While this is generally a good assumption when the concentration of CCN is low (e.g., when size-resolved CCN experiments using a DMA are carried out), the extent of these depletion effects at higher CCN concentrations have not been systematically quantified to date. This is especially important for CCN studies in polluted environments (or other conditions of high CCN). Water vapor depletion effects can also affect the final activated droplet size, which can bias studies of activation kinetics carried out with the CFSTGC. This study aims at understanding and quantifying water vapor depletion effects on

supersaturation and droplet growth in the CFSTGC using a comprehensive combination of instrument theoretical analysis and laboratory activation experiments.

2. Theory of water vapor depletion effects

We first proceed with a simple scaling analysis to determine when water vapor depletion in the instrument can impact supersaturation and droplet size at the exit of the chamber. For this, we first determine the "zero CCN" limit of supersaturation and droplet growth (corresponding to very small CCN concentrations flowing through the instrument). The perturbation about the "zero CCN" limit is then determined as a function of chamber CCN concentration (and other relevant variables, such as flow rate and streamwise temperature gradient) to express depletion effects. In the analysis, we assume that air flows with a total rate Q through the growth chamber of radius R and wall temperature gradient G. We also assume that supersaturation depletion is primarily from condensational loss of water vapor to the CCN; the release of latent heat has a second order impact on supersaturation (numerical simulations in section 3 confirm this).

Depletion effects on supersaturation

The saturation ratio, $S = \frac{P}{P_s}$, of a fluid "material point" flowing along the centerline of the chamber (P, P_s are the partial and saturation pressure of water, respectively) can change over time as follows:

$$\frac{dS}{dt} = \frac{d}{dt}\left(\frac{P}{P_s}\right) = \frac{1}{P_s}\frac{dP}{dt} - \frac{P}{P_s^2}\frac{dP_s}{dt} = \frac{1}{P_s}\left[\frac{dP}{dt} - S\frac{dP_s}{dt}\right] \quad (1)$$

where d/dt denotes the material (or Lagrangian) derivative of a material point property. Equation (1) expresses the change in saturation ratio from fluctuations in water vapor

concentration (P) and temperature (P_s). From the chain rule, $\frac{dP_s}{dt} = \frac{dP_s}{dT}\frac{dT}{dz}\frac{dz}{dt}$; assuming $\frac{dT}{dz} = G$, $\frac{dz}{dt}$ is the average flow velocity $\sim \frac{Q}{\pi R^2}$ [Roberts and Nenes, 2005], and, $\frac{dP_s}{dT} = \frac{\Delta H_v P_s}{R_g T^2}$ from the Clausius-Clapeyron Equation (where T is the temperature and ΔH_v, R_g are the enthalpy of evaporation and specific gas constant for water, respectively) we obtain:

$$\frac{dP_s}{dt} = \frac{\Delta H_v P_s}{R_g T^2} G \frac{Q}{\pi R^2} \tag{2}$$

Substitution of Eq. (2) into Eq. (1) gives:

$$\frac{dS}{dt} = \frac{1}{P_s}\left[\frac{dP}{dt} - \frac{\Delta H_v P_s}{R_g T^2} G \frac{Q}{\pi R^2} S\right] \tag{3}$$

$\frac{dP}{dt}$ can be expressed as the sum of water vapor supply from transport, $\dot{S}$, and condensational loss, $\dot{C}$, from the activated CCN:

$$\frac{dS}{dt} = \frac{1}{P_s}\left[\dot{S} - \dot{C} - \frac{\Delta H_v P_s}{R_g T^2} G \frac{Q}{\pi R^2} S\right] \tag{4}$$

When the concentration of CCN, N, approaches zero, then $\dot{C} \to 0$; assuming the flow field is also developed, $\frac{dS}{dt} \simeq 0$ and Equation (4) becomes:

$$\dot{S} = \frac{\Delta H_v P_s}{R_g T^2} G \frac{Q}{\pi R^2} S_o \tag{5}$$

where S_o denotes the maximum (or "effective") saturation ratio in the instrument for "zero CCN" conditions (determined from instrument calibration; Section 4).

$\dot{S}$ is controlled by the transport of water vapor from the chamber walls, and should not depend on N. Hence, Equation (5) can be substituted into (4) to give the general supersaturation depletion equation:

$$\frac{dS}{dt} = \frac{\Delta H_v G Q}{\pi R^2 R_g T^2}\left(S_o - S\right) - \frac{\dot{C}}{P_s} \tag{6}$$

If S along a streamline is assumed to be in a dynamical steady-state, $\frac{dS}{dt} \simeq 0$. With this and expressing the saturation ratio in terms of supersaturation ($S = s+1$ and $S_o = s_o+1$), Equation (6) becomes:

$$s = s_o - \frac{\pi R^2 R_g T^2}{\Delta H_v G Q P_s}\dot{C} \tag{7}$$

Equation (7) expresses the supersaturation depletion (in the developed flow region of the chamber) from the condensational growth of activated CCN.

Depletion effects on droplet size at the exit of the growth chamber

The average size of activated CCN, D_p, at the exit of the growth chamber (which experimentally is measured in the optical particle counter of the CFSTGC) is taken as the characteristic diameter for expressing droplet size reduction in our analysis. D_p can be obtained from the integration of the droplet growth equation [Seinfeld and Pandis, 2006] over the particle residence time in the instrument [Roberts and Nenes, 2005]:

$$D_p^2 = D_c^2 + 2\int_{\tau} \Gamma s(t) dt \tag{8}$$

where D_c , τ are the characteristic critical wet diameter and the residence time of the CCN in the instrument, respectively. $s(t)$ denotes the streamwise supersaturation profile that particles are exposed to while flowing in the growth chamber. Γ is a growth parameter that depends on droplet size and the water vapor mass transfer coefficient [e.g., Seinfeld and Pandis, 2006; Nenes and Seinfeld, 2003].

Assuming Equation (7) applies at every point in the axial direction, it can be introduced into (8) to give:

$$D_p^2 = D_c^2 + 2\int_\tau \Gamma s_o(t)dt - 2\int_\tau \Gamma \frac{\pi R^2 R_g T^2}{\Delta H_v GQP_s}\dot{C}dt \tag{9}$$

where $s_o(t)$ denotes the supersaturation profile at "zero CCN" concentration (corresponding to the instrument "steady-state" supersaturation; Roberts and Nenes, 2005; Lance et al., 2006).

The average droplet size at "zero CCN" concentration, $D_{po} = \left(D_c^2 + 2\int_\tau \Gamma s_o dt \right)^{1/2}$, is given by Equation (9) for $\dot{C} \to 0$. When higher concentrations of CCN flow in the chamber, water vapor depletion leads to a lower s, hence lower D_p than D_{po}:

$$D_p^2 = D_{po}^2 - 2\int_\tau \Gamma \frac{\pi R^2 R_g T^2}{\Delta H_v GQP_s}\dot{C}dt \tag{10}$$

Simplified expressions for condensation effects on s, D_p

Equations (7) and (10) give the impact of CCN growth on supersaturation and droplet size at the exit of the growth chamber; more convenient forms can be derived if $\dot{C}$ is explicitly written in terms of D_p, N and Γ. Assuming that the droplets formed can be

divided into n classes of concentration N_i and wet diameter D_{pi} (that increases in the streamwise direction), $\dot{C}$ can be expressed at a given point in the flow chamber as

$$\dot{C} = \frac{dP}{dt} = \frac{R^* T \rho_w}{M_w} \frac{d}{dt}\left[\frac{\pi}{6}\sum_n N_i D_{pi}^3\right] = \frac{\pi}{2}\frac{R^* T \rho_w}{M_w}\sum_n N_i D_{pi}^2 \frac{dD_{pi}}{dt} \tag{11}$$

where R^*, M_w, ρ_w are the universal gas constant, the molar mass and density of liquid water, respectively. From the droplet growth equation [Roberts and Nenes, 2005], $\frac{dD_{pi}}{dt} = \frac{\Gamma s}{D_{pi}}$; with this and the definition of average droplet size $\bar{D}_p = \frac{1}{N}\sum_n N_i D_{pi}$, Equation (11) becomes

$$\dot{C} = \frac{\pi}{2}\frac{R^* T \rho_w}{M_w}\Gamma N \bar{D}_p s \tag{12}$$

Combination of Equations (12) and (7) eventually gives

$$\frac{s}{s_o} = \frac{1}{1 + \frac{\Phi}{2}\Gamma N \bar{D}_p} \tag{13}$$

where $\Phi = \frac{\pi^2 R^2 R_g R^* T^3 \rho_w}{\Delta H_v G Q P_s M_w}$. Applying the binomial expansion up to first order, $(1+x)^{-1} \simeq 1 - x$, Equation (13) is approximated by:

$$\frac{s}{s_o} \simeq 1 - \frac{\Phi}{2}\Gamma N \bar{D}_p \tag{14}$$

To express the depression in instrument (i.e., maximum) supersaturation, Equation (14) should be applied in the vicinity of the supersaturation entry length [Lance et al., 2006], where all the CCN have activated but experienced the least amount of growth. Further

downwind in the chamber, Equation (14) still applies but predicts increasingly larger supersaturation depletion because $\bar{D}_p$ increases by condensation of water vapor. In fact, Equation (14) suggests that supersaturation decreases downwind of its maximum value as $\frac{ds}{dz} \simeq s_o \frac{\Phi}{2} \Gamma N \frac{d\bar{D}_p}{dz}$.

Simplification of the droplet size depression equation results from combination of Equations (12) and (10):

$$D_p^2 = D_{po}^2 - \int_\tau \Phi \Gamma^2 N \bar{D}_p s dt = D_{po}^2 - \Phi \Gamma^2 N \int_\tau \bar{D}_p s dt \tag{15}$$

Defining the column-average droplet size, $\bar{\bar{D}}_p = \frac{\int_\tau \bar{D}_p s dt}{\int_\tau s dt}$, then $\int_\tau \bar{D}_p s dt = \bar{\bar{D}}_p \int_\tau s dt$ and Equation (15) becomes:

$$D_p^2 = D_{po}^2 - \Phi \Gamma^2 N \bar{\bar{D}}_p \int_\tau s dt \simeq D_{po}^2 - \frac{\Phi}{2} \Gamma N \bar{\bar{D}}_p D_p^2 \tag{16}$$

where $D_p^2 \simeq 2 \int_\tau \Gamma s dt$ (a valid approximation for CCN that exhibit considerable growth beyond their critical wet diameter, i.e., $D_c^2 \ll 2 \int_\tau \Gamma s dt$; Nenes and Seinfeld, 2003).

Manipulation of Equation (16) gives

$$\frac{D_p}{D_{po}} = \left(1 + \frac{\Phi}{2} \Gamma N \bar{\bar{D}}_p \right)^{-1/2} \simeq 1 - \frac{\Phi}{4} \Gamma N \bar{\bar{D}}_p \tag{17}$$

where the truncated expansion $(1+x)^{-1/2} \simeq 1 - \frac{x}{2}$ is used.

Equations (14) and (17) are remarkably similar. Both expressions would exhibit identical dependence on N, Φ and Γ (hence imply that $\frac{s}{s_o} \simeq \frac{D_p}{D_{po}}$) if $\bar{\bar{D}}_p \simeq 2\bar{D}_p$. Numerical simulations (Section 3) and experimental observations (Section 4) suggest this is often the case.

3. Instrument and Droplet Growth Models

The CFSTGC instrument model [Roberts and Nenes 2005; Lance et al., 2006] numerically integrates the Navier-Stokes equations and the heat and water vapor conservation equations to predict the velocity, pressure, water vapor supersaturation, and temperature fields in the instrument. The model has been shown to successfully simulate instrument behavior over a wide range of operating conditions [Lance et al. 2006; Rose et al. 2008]. Inputs to the model are total volumetric flow rate (Q), sheath-to-aerosol flow ratio (SAR), pressure (P), and the inner wall streamwise temperature gradient (G) between the exit and entrance of the column. The simulated supersaturation, velocity, and temperature profiles are used to compute the activation and growth of CCN (with a user-defined size distribution and composition) as they flow through the chamber. Integration of the CCN growth equations is accomplished with the LSODE (Livermore Solver for ODEs) solver [Hindmarsh 1983]. The loss of water vapor from the gas phase onto the growing CCN and associated latent heat are then allowed to affect the gas phase water vapor and heat balances [Nenes et al. 2001; Roberts and Nenes 2005]. For more details about the modeling framework, the solution algorithm and the instrument characteristics, refer to Roberts and Nenes [2005] and Lance et al., [2006].

To study supersaturation depletion effects, we vary the temperature gradient, total flow rate, pressure, aerosol concentration, size distribution characteristics, and, the water vapor uptake coefficient for the combinations of these parameters given in Table 1. The flow field in the growth chamber is discretized onto 100 grid points in the streamwise direction and 100 grid points in the radial direction. The temperature of the air (both sheath and aerosol flows) entering the column is 293 K and the sheath-to-aerosol ratio in the growth chamber is 10:1. Aerosol flows through the instrument that follows a single lognormal mode of ammonium sulfate aerosol with a geometric mean dry diameter, D_g, of 0.04-0.1 μm, geometric standard deviation, σ_g, of 1.6, and number concentration, N_a, between 1 and 2×10^4 cm^{-3}. The size distribution is discretized onto 50 bins equally spaced in log-size between 20 nm and 1 μm. The water vapor uptake coefficient, α_c, (used in Γ to express differences in activation kinetics of the CCN) was varied between 0.01 and 1.0, which represents the range of activation kinetics observed to date in carbonaceous and atmospheric aerosol [e.g., Ruehl et al., 2008, 2009; Asa-Awuku et al., 2009]. A total of over 1100 simulations were completed.

Figure 1 presents a typical example of the effects of CCN on instrument supersaturation and temperature. Shown are predicted centerline supersaturation and temperature profiles in the CFSTGC for different levels of aerosol concentration. Chamber conditions correspond to Q = 0.5 L min^{-1}, wall temperature gradient 16 Km^{-1} (i.e., a 8K difference between the entry and exit of the growth chamber) and 1000 mb chamber pressure. Aerosol is assumed to be composed of $(NH_4)_2SO_4$, with D_g = 100nm, σ_g = 0.16 and α_c = 1. The thickness of the temperature profile line represents the variability of the quantity across simulations, arising from latent heat released by the water vapor condensing upon

the growing droplets. The temperature profile is largely unaffected by the aerosol up to concentrations of 10^4 cm^{-3} (maximum temperature increase of 0.07K), with a negligible impact on the streamwise temperature gradient and supersaturation (less than 2% relative change compared to "zero CCN" conditions). The supersaturation profile for the lowest aerosol concentration (1 cm^{-3}) corresponds to the "zero CCN" solution; supersaturation develops after passing of its characteristic entry length [Lance et al., 2006], reaches a maximum value (~ 0.33%) and slowly decays from the effects of increasing the absolute temperature in the streamwise direction [Roberts and Nenes, 2005]. Increasing the CCN concentration above 1000 cm^{-3} begins to impact the supersaturation profile. Consistent with the scaling analysis of Section 2, both maximum supersaturation and its decay are equally affected. However, the location of the maximum in the instrument is not affected, so that the length of chamber available for growth is unaffected by the CCN concentration level.

A change in supersaturation is expected to induce a change in the size of droplets exiting the column. This is shown in Figure 2, which presents the predicted centerline droplet diameter as a function of distance from the chamber inlet for the simulations of Figure 1. Clearly, the "zero CCN" simulation provides the largest droplet sizes; increasing CCN concentrations depresses droplet size by more than 30% at the exit of the chamber. Also shown in the inset graph is the droplet relative dispersion (defined as the width of the droplet distribution normalized by the average diameter); it decreases in the flow direction, consistent with the diffusional narrowing expected for the droplets during their residence in the chamber. Despite the variation of average droplet diameter and relative dispersion with CCN concentration, the former tend to be uniquely correlated. This

suggests that the droplet size distribution is strongly linked to the level of supersaturation that eventually develops in the CFSTGC (regardless if depletion effects are important).

Figure 3 presents the predicted supersaturation depletion (left panels) and droplet size depression ratios (right panels) as a function of CCN concentration (defined as the droplet concentration exiting the flow chamber in each simulation). Each panel shows simulations for Q = 0.5 L min^{-1}, wall temperature gradient 8, 16 K m^{-1}, chamber pressure 500, 750, 1000 mb and $(NH_4)_2SO_4$ aerosol with D_g = 40,100nm, σ_g=0.19 and N_a from 1 to 2×10^4 cm^{-3}. Results are shown for α_c=1 (Panels a, b), α_c=0.06 (Panels c, d), and α_c=0.01 (Panels e, f). The behavior seen in all these plots are consistent with the analysis of Section 2, as both s/s_o and D_p/D_{po} scale linearly with N, with remarkably similar slopes. The diverse set of instrument operating conditions and aerosol characteristics considered in the simulations introduce a relatively small variability in s/s_o and D_p/D_{po}; this implies that changes in G, Q induce responses in $\bar{D}_p$, $\bar{\bar{D}}_p$ so that $\Phi\bar{D}_p \simeq const.$ (Equation 17). The sensitivity to α_c however is important; a lower value of the parameter tends to reduce the intensity of supersaturation depletion effects. This is expected because reduction of α_c reduces Γ, hence s/s_o and D_p/D_{po} at constant N (Equations 14,17). Based on Figure 3, a 10% reduction in s and D_p is predicted for $N \sim 4\times10^3$ for rapidly activating aerosol (α_c=1), $N \sim 10^4$ for intermediate (α_c=0.06), and $N \sim 3.5\times10^4$ for slowly activating aerosol (α_c=0.01).

Given that the "supply" rate of water vapor in the instrument is constrained by the operation conditions (G, transport timescale of water vapor), condensational effects can only act to reduce the s profile in the flow chamber. This means that if condensational

depletion of supersaturation notably affects outlet droplet sizes, it will also affect the maximum (hence effective) supersaturation in the instrument. The simulations (Figure 3) and theoretical analysis strongly supports this. Furthermore, while the presence of water vapor depletion may affect the shape of the supersaturation profile somewhat (Figure 1), the strongest effect on outlet droplet size arises from the reduction in effective supersaturation (i.e., the magnitude of the maximum). This is clearly shown in Figure 4, which shows the average droplet diameter predicted at the exit of growth chamber vs. supersaturation (with depletion effects considered) for the range of Q, α_c, N_a and D_g presented in Table 1. If water vapor depletion significantly affected the shape of the supersaturation profile in the instrument, it would also change the relationship between s and D_p (keeping Q, a_c and D_g constant). This however is not the case, as simulations corresponding to "zero CCN" conditions (N_a < 500 cm^{-3}; filled triangles) follow the same s vs. D_p relationship as for simulations with high N_a.

4. Experimental Determination of Depletion Effects

To experimentally determine supersaturation depletion and outlet droplet size depression, we carry out two types of experiments: a "standard" instrument calibration (such as those described in Lance et al., 2006; Rose et al., 2008) to determine the supersaturation. We then proceed with polydisperse CCN activation experiments to quantify the effects of water vapor depletion on supersaturation and droplet size. In all experiments we use $(NH_4)_2SO_4$ aerosol, generated by atomization of an aqueous solution of the salt.

The instrumentation setup used to determine the "zero CCN" supersaturation level in the instrument is shown in Figure 5a. Polydisperse dry aerosol is charge-neutralized using a Po-210 neutralizer and introduced into a differential mobility analyzer (DMA, TSI

3081L) for size classification by electrical mobility. The classified aerosol is then split between a condensation particle counter (CPC, TSI 3010) for measurement of total aerosol (condensation nuclei, CN) concentration, and a Droplet Measurement Technologies Continuous-Flow CFSTGC (serial number 002) to measure CCN concentrations. In order to maintain a sample flow rate of 1 LPM through the DMA, filtered air is supplied to the classified aerosol stream or to the CPC stream (the latter being preferable in cases where low aerosol concentrations limit the counting statistics in the CFSTGC). In this study, the aerosol classification is operated as in a Scanning Mobility Particle Sizer [SMPS; Wang and Flagan, 1989], where the voltage applied to the DMA is exponentially scanned over time. The TSI Aerosol Instrument Manager control software is used to scan the voltage, manage data acquisition in the CPC and carry out the inversion to provide the aerosol number size distribution. The timeseries of CN and CCN counts obtained during a voltage ramp is then inverted into a "CCN activation curve" using SMCA [Moore et al., 2010] which provides the ratio of particles that are CCN-active as a function of their dry mobility diameter. The critical supersaturation (using Köhler theory) of the particle with dry diameter, d_{50} (at which 50% of the classified aerosol act as CCN) is then used to characterize the instrument supersaturation:

$$s_c = \left(\frac{4A^3}{27B} \right)^{1/2} \tag{18}$$

where $A = \frac{4M_w\sigma}{R^*T\rho_w}$, $B = \frac{\varphi_s \nu_s \rho_s d_s^3}{\rho_w M_w}$, σ is the droplet-air surface tension at the point of activation, and, φ_s, ν_s, and ρ_s are the osmotic coefficient, stoichiometric van't Hoff factor, and density of the solute, respectively. φ_s accounts for the incomplete solute dissociation and

was calculated for $(NH_4)_2SO_4$ using the ion-interaction approach of Pitzer and Mayorga [1973] with parameters taken from Clegg and Brimblecombe [1988]. This supersaturation calibration procedure is repeated for a range of instrument operating conditions (column temperature gradient, flow rate and column pressure). The particle concentration in the CFSTGC during SMCA (generally less than 500 cm^{-3}) is low enough for water vapor depletion effects to be negligible; hence the calibrated supersaturation corresponds to the "zero CCN" supersaturation levels.

The polydisperse activation experiments are completed using the experimental setup shown in Figure 5b; polydisperse aerosol is generated with an atomizer and dried by a series of diffusional dryers. The aerosol stream is then sampled by a SMPS and the CFSTGC. The flow rate in the instrument was kept at Q = 0.5 L min^{-1}, ambient pressure 980 mb, and several temperature gradients corresponding to a "zero CCN" supersaturation range between 0.23% and 0.62%. The concentration and size distribution of the aerosol is varied by changing the atomizer pressure and concentration of salt solution placed in the atomizer. A single-mode aerosol is typically generated that is well-described with a lognormal distribution, with $\sigma_g = 0.16$, D_g varying between 40nm and 70nm, and, N_a ranging from ~5×10^2 to 5×10^4 cm^{-3}. Supersaturation depletion effects in the CFSTGC are quantified by determining the effective supersaturation in the instrument for each CCN concentration level measured. This is done by determining the characteristic dry size, d^*, for which integration of the SMPS size distribution (from d^* to the highest resolved diameter, ~300nm) matches the average CCN concentration observed during the SMPS scan. d^* is then used to characterize the instrument supersaturation, s, (through application of Equation 18) from which s/s_o is calculated.

Droplet growth depletion is quantified by calculating the average droplet size measured by the instrument OPC as a function of the total CCN concentration, normalized with the "zero CCN" droplet size (also determined from polydisperse activation experiments, under conditions of low particle concentration, less than 500 cm^{-3}).

Results of the polydisperse activation experiments are presented in Figure 6. Panel a presents measured droplet size depression ratios, D_p/D_{po}, as a function of CCN concentration. All the activation experiments conducted collapse onto a narrow band that follows a linear trend; the slope of D_p/D_{po} vs. N (-2.53×10^{-5} cm^3) is close to the numerical predictions for aerosol with α_c=1.0 (-1.90×10^{-5} cm^3; Figure 3b). When measured droplet depression ratio is placed against predictions (Figure 6b), an excellent agreement can be obtained; even extrapolation of the simulations to higher CCN concentrations fits the experimental data well.

Figure 6c presents the supersaturation depletion as a function of CCN concentration in the instrument. Consistent with simulations, the activation experiments collapse onto a narrow band that follows a linear trend; the slope of s/s_o vs. N (-1.94×10^{-5} cm^3) is close to the numerical predictions for aerosol with α_c=1.0 (-2.01×10^{-5} cm^3; Figure 3a). Finally, the average droplet diameter measured by the instrument OPC vs. supersaturation (with depletion effects considered) is shown in Figure 6d. In agreement with simulations (Figure 4), the relationship between s and D_p is not affected by the level of CCN in the instrument, as "zero CCN" observations (i.e., N_a < 500 cm^{-3}; filled triangles) follow the same curve as for measurements at high CCN concentration.

All the evidence presented above strongly suggests that the theoretical analysis presented in sections 2 and 3 is a realistic representation of water vapor depletion effects in the

CFSTGC. Against initial expectations, the coupling of supersaturation, CCN number and outlet droplet size gives rise to a remarkably simple relationship between supersaturation and droplet size depletion. This is shown in Figure 7, which presents s/s_o vs D_p/D_{po} from the simulations (panel a) and the observations (panel b). For the wide range of conditions considered, $\frac{s}{s_o} \simeq \frac{D_p}{D_{po}}$ to within 10%.

The analysis presented does not consider the effect of coincidence errors for measurements of CCN at high concentrations; for the instrumentation used, a maximum coincidence error of 10% can occur for concentrations up to 6000 cm^{-3} [DMT, 2005]. The consistency between the theoretical analysis and instrument observations suggests that coincidence errors, if present, constitute a secondary effect on the observed instrument response.

6. Summary and Implications.

All published studies with the Continuous-Flow Streamwise Thermal Gradient Chamber assume that the supersaturation generated in the instrument is not influenced by the condensation of water vapor upon the growing CCN. This study evaluates this assumption and examines the conditions for which depletion effects become important for supersaturation, measured CCN concentration and droplet growth. An analysis is carried out with a fully coupled numerical model and laboratory CCN activation experiments using a commercial instrument.

We find that condensational depletion of water vapor does not impact supersaturation and droplet size by more than 10% (which is comparable to the supersaturation uncertainty quoted for the CFSTGC [e.g., Rose et al., 2008]) if the CCN are present at concentrations

below 5000 cm^{-3}. If the CCN exhibit slower activation kinetics than $(NH_4)_2SO_4$ aerosol, higher concentrations can be present in the instrument before depletion effects become important. Remarkably, depletion effects do not significantly alter the shape of the supersaturation distribution in the instrument growth chamber, so that the relationship between instrument supersaturation and outlet droplet size does not change (regardless of the extent of supersaturation depletion). The above suggests that the majority of atmospherically-relevant CCN measurements with the DMT CFSTGC may not be substantially affected by supersaturation depletion. However, high CCN concentrations can occur with enough frequency (especially if sampling polydisperse CCN in polluted environments, or in laboratory experiments with high particulate loads) that a methodology needs to be developed to address the issue.

There are a number of approaches that can be used to eliminate biases from supersaturation depletion. One approach is to avoid depletion effects all together by maintaining a low concentration of CCN in the instrument during laboratory calibrations and atmospheric sampling. Low concentrations of CCN can be achieved in-situ by either performing size-resolved CCN measurements (e.g. SMCA) or through controlled dilution of the sample stream with filtered air before entering the CFSTGC. Another approach is to account for depletion biases using the relationship of s/s_o versus CCN presented in this manuscript; the effective supersaturation then corresponds to the measured CCN level and droplet size – and is equivalent to measurements carried out under "zero CCN conditions". The degree of correction is sensitive to the activation kinetics of the ambient aerosol, but an analysis with the instrument model (such as carried out in this manuscript) can largely account for this uncertainty. Supported by the available body of evidence [e.g.,

Bougiatioti et al., 2009; Lance et al., 2009; Ruehl et al., 2008, 2009], rapid activation kinetics (i.e., α_c comparable to that of $(NH_4)_2SO_4$ aerosol ~ 0.1) can be assumed *a priori* when the aerosol is aged, sampled from a humid environment or contains large amounts of soluble material.

The analysis carried out here can be extended to the different operation modes and implementations of the CFSTGC design [e.g., Ruehl et al., 2008, Moore et al., 2010] or any other CCN instrument design (such as those analyzed in Nenes et al., 2001). Regardless of the method used to measure CCN concentrations, this study shows that depletion effects need to be carefully understood for unambiguous measurements of CCN activity and droplet activation kinetics.

Acknowledgments

We would like to thank R. Moore for comments that improved the manuscript. We acknowledge funding from NSF CAREER, NOAA, an NSF Graduate Student Fellowship and a Georgia Institute of Technology Presidential Scholarship.

References

Asa-Awuku, A., G. Engelhart, B. Lee, S. Pandis, and A. Nenes (2009) Relating CCN activity, volatility, and droplet growth kinetics of β-caryophyllene secondary organic aerosol, *Atmos. Chem. Phys.*, 9, 795–812.

Asa-Awuku, A., A. Nenes, S. Gao, R. Flagan, and J. Seinfeld (2010) Water-soluble SOA from Alkene ozonolysis: composition and droplet activation kinetics inferences from analysis of CCN activity, *Atmos. Chem. Phys.*, 10, 1585-1597.

Bougiatioti, A., C. Fountoukis, N. Kalivitis, S. Pandis, A. Nenes, and N. Mihalopoulos (2009) Cloud condensation nuclei measurements in the marine boundary layer of the Eastern Mediterranean: CCN closure and droplet growth kinetics, *Atmos. Chem. Phys.*, 9, 7053–7066.

Clegg, S. L., and P. Brimblecombe (1988) Equilibrium partial pressures of strong acids over concentrated saline solutions - I. HNO_3, *Atmos. Environ.*, 22, 91–100.

Chuang, P.Y. (2006) Sensitivity of cloud condensation nuclei activation processes to kinetic parameters, *J. Geoph. Res.*, 111, D09201.

Cubison, M., B. Ervens, G. Feingold, K. Docherty, I. Ulbrich, L. Shields, K. Prather, S. Hering, and J. Jimenez (2008) The influence of chemical composition and mixing state of Los Angeles urban aerosol on CCN number and cloud properties, *Atmos. Chem. Phys.*, 8, 5649–5667.

Droplet Measurement Technologies (DMT), Cloud Condensation Nuclei Counter Operator Manual, Rev. A, March 2005.

Engelhart, G., A. Asa-Awuku, A. Nenes, and S. N. Pandis (2008) CCN activity and droplet growth kinetics of fresh and aged monoterpene secondary organic aerosol, *Atmos. Chem. Phys.*, 8, 3937–3949.

Hindmarsh, A. (1983) ODEPACK: A systematized collection of ODE solvers, in *Scientific Computing*, edited by Stepleman et al., and North-Holland, New York, 55–64.

Kuwata, M., Y. Kondo, Y. Miyazaki, Y. Komazaki, J. H. Kim, S. S. Yum, H. Tanimoto, and H. Matsueda (2008) Cloud condensation nuclei activity at Jeju Island, Korea in spring 2005, *Atmos. Chem. Phys.*, 8, 2933–2948.

Lance, S. (2007) Quantifying compositional impacts of ambient aerosol on cloud droplet formation, Ph.D. thesis, Georgia Institute of Technology, Atlanta, GA.

Lance, S., J. Medina, J. Smith, and A. Nenes (2006) Mapping the operation of the DMT continuous flow CCN counter, *Aerosol Sci. Technol.*, 40, 242–254.

Lance, S., A. Nenes, C. Mazzoleni, M. Dubey, H. Gates, V. Varutbangkul, T. A. Rissman, S. M. Murphy, A. Sorooshian, F. Brechtel, R. Flagan, J. Seinfeld, G. Feingold, and H.

Jonsson (2009) CCN activity, closure and droplet growth kinetics of Houston aerosol during the Gulf of Mexico Atmospheric Composition and Climate Study (GoMACCS), *J. Geophys. Res.*, (D00F15), 114.

Moore, R., and A. Nenes (2009) Scanning flow CCN analysis - a method for fast measurements of CCN spectra, *Aerosol Sci. Technol.*, 43, 1192–1207.

Moore., R., Nenes, A., and Medina, J. (2010) Scanning Mobility CCN Analysis - A method for fast measurements of size resolved CCN distributions and activation kinetics, *Aeros.Sci.Technol.*, 44, 861-871.

Murphy, S.M., Agrawal, H., Sorooshian, A., Padro, L.T., Gates, H., Hersey, S., Welch, W.A., Jung, H., Miller, J.W., Cocker, D.R., Nenes, A., Jonsson, H., Flagan, R.C., and Seinfeld, J.H. (2009) Comprehensive Simultaneous Shipboard and Airborne Characterization of Exhaust from a Modern Container Ship at Sea, *Env.Sci.Tech.*, 43, 4626-4640.

Nenes, A., and J. H. Seinfeld (2003) Parameterization of cloud droplet formation in global climate models, J. Geophys. Res., (D7), doi: 10.1029/2002JD002, 911.

Nenes, A., P. Chuang, R. Flagan, and J. Seinfeld (2001) A theoretical analysis of cloud condensation nucleus (CCN) instruments, *J. Geophys. Res.*, 106, 3449–3474.

Padró, L., A. Asa-Awuku, R. Morrison, and A. Nenes (2007) Inferring thermodynamic properties from CCN activation experiments: Single-component and binary aerosols, *Atmos. Chem. Phys.*, 7, 5263–5274.

Petters, M., and S. Kreidenweis (2007) A single parameter representation of hygroscopic growth and CCN activity, *Atmos. Chem. Phys.*, 7, 1961–1971.

Petters, M., C. Carrico, S. Kreidenweis, A. Prenni, P. DeMott, J. C. Jr., and H. Moosmuller (2009) Cloud condensation nucleation activity of biomass burning aerosol, *J. Geophys. Res.*, 114, D22,205.

Pitzer, K., and G. Mayorga (1973) Thermodynamics of electrolytes. II. activity and osmotic coefficients for strong electrolytes with one or both ions univalent, *J. Phys. Chem.*, 77, 2300–2308.

Roberts, G., and A. Nenes (2005) A continuous-flow streamwise thermal-gradient CCN chamber for atmospheric measurements, *Aerosol Sci. Technol.*, 39, 206–221.

Roberts, G.C., Day, D.A., Russell, L.M., Dunlea, E.J., Jimenez, J.L., Tomlinson, J.M., Collins, D.R., Shinozuka, Y., and Clarke, A.D. (2010) Characterization of particle cloud droplet activity and composition in the free troposphere and the boundary layer during INTEX-B, *Atmos. Chem. Phys.*, 10, 6627–6644

Rose, D., S. Gunthe, E. Mikhailov, G. Frank, U. Dusek, M. Andreae, and U. Pöschl (2008) Calibration and measurement uncertainties of a continuous-flow cloud condensation nuclei counter (DMT-CCNC): CCN activation of ammonium sulfate and sodium chloride aerosol particles in theory and experiment, *Atmos. Chem. Phys.*, 8, 1153–1179.

Rose, D., A. Nowak, P. Achtert, A. Wiedensohler, M. Hu, M. Shao, Y. Zhang, M. Andreae, and U. Pöschl (2010) Cloud condensation nuclei in polluted air and biomass burning smoke near the mega-city Guangzhou, China - Part 1: Size-resolved measurements and implications for the modeling of aerosol particle hygroscopicity and CCN activity, *Atmos. Chem. Phys.*, 10, 3365–3383.

Ruehl, C. P., C.R., and A. Nenes (2008) How quickly do cloud droplets form on atmospheric particles?, *Atmos. Chem. Phys.*, 8, 1043–1055.

Ruehl, C., P. Chuang, and A. Nenes (2009) Distinct CCN activation kinetics above the marine boundary layer along the California coast, *Geophys. Res. Lett.*, 36 :L15814.

Seinfeld, J., and S. Pandis (2006) *Atmospheric chemistry and physics: from air pollution to climate change*, 2nd ed., John Wiley, New York.

Sorooshian, A., Murphy, S.M., Hersey, S., Gates, H., Padro, L.T., Nenes, A., Brechtel, F.J., Jonsson, H., Flagan, R.C. and Seinfeld, J.H. (2008) Comprehensive airborne characterization of aerosol from a major bovine source, *Atmos. Chem. Phys.*, 8, 3937-3949

Wang, S., and Flagan, R. (1989) Scanning Electrical Mobility Spectrometer, *J.*

Aerosol Sci., 20, 1485–1488

Wex, H., T. Hennig, I. Salma, R. Ocskay, A. Kiselev, S. Henning, A. Massling, A. Wiedensohler, and F. Stratmann (2007) Hygroscopic growth and measured and modeled critical supersaturations of an atmospheric HULIS sample, *Geophys. Res. Lett.*, doi: 10.102/2006GL028, 260.

Table 1: Operating conditions and aerosol characteristics considered in the CFSTGC instrument simulations.

Property	Values considered
Instrument conditions	
P (mb)	1000, 750, 500
G (K m^{-1})	6, 8, 11, 16*
Q (L m^{-1})	0.5, 1.0
Aerosol properties	
D_g (nm)	40, 100
σ_g	1.6
N_a (cm^{-3})	1, 5×10^2, 10^3, 5×10^3, 10^4, 2×10^4, 3×10^4, 5×10^4
α_c	1.0, 0.06, 0.01

***** i.e., inlet-outlet temperaure difference of 3, 4, 5.5., 8K respectively.

Figure Captions

Figure 1: Predicted centerline temperature (black line) and supersaturation (symbols) profiles in the CFSTGC for different levels of aerosol flowing through the instrument. Chamber conditions correspond to Q = 0.5 L min^{-1}, wall temperature gradient 16 Km^{-1} and 1000 mb chamber pressure. Aerosol is composed of $(NH_4)_2SO_4$, and follows a lognormal distribution with 100 nm modal diameter and 0.16 geometric standard deviation. α_c is assumed unity. The thickness of the temperature profile line represents the variability across all simulations.

Figure 2: Predicted centerline droplet diameter and relative dispersion (inset graph) in the CFSTGC for different levels of aerosol flowing through the instrument. Chamber and aerosol characteristics are identical to those of Figure 1.

Figure 3: Predicted supersaturation depletion (left panels) and droplet size depression ratios (right panels) as a function of CCN concentration (defined as the droplet concentration exiting the flow chamber). Results shown for α_c=1 (Panels a, b), α_c=0.06 (Panels c, d), and α_c=0.01 (Panels e, f). Each panel shows simulations for Q = 0.5 L min^{-1}, wall temperature gradient 8, 16 K m^{-1}, chamber pressure 500, 750, 1000 mb and $(NH_4)_2SO_4$ aerosol following a lognormal distribution with 40, 100 nm modal diameter, 0.19 geometric standard deviation and total concentration from 1 to 2×10^4 cm^{-3}.

Figure 4: Predicted average droplet diameter at the exit of growth chamber vs. supersaturation (with depletion effects considered) for Q=0.5 L min^{-1}, α_c=1 (Panel a), Q=0.5 L min^{-1}, α_c=0.06 (Panel b), Q=1.0 L min^{-1}, α_c=0.06 (Panel c), and Q=0.5 L min^{-1}, α_c=0.01 (Panel d). Triangles denote simulations that correspond to "zero CCN" conditions (defined as aerosol concentration below 500 cm^{-3}).

Figure 5: Instrument setup for (a) "zero CCN" instrument supersaturation calibration, and, (b) polydisperse CCN activation experiments.

Figure 6: Measured CFSTGC responses to increasing levels of CCN in the flow chamber. Instrument operation was kept at Q = 0.5 L min^{-1}, chamber pressure 980 mb and

$(NH_4)_2SO_4$ aerosol following a lognormal distribution with 40, 70 nm modal diameter, 0.2 geometric standard deviation and total concentration from 1 to ~ 3×10^4 cm^{-3}. (a) droplet size depression ratios as a function of CCN concentration (b) Predicted vs. measured droplet size depression ratios as a function of CCN concentration, for Q = 0.5 L min^{-1}, P= 980 mb and s_o = 0.62% (α_c=1.0 is assumed in the simulations). (c) Measured supersaturation depletion as a function of CCN concentration. (d) average droplet size measured at the optical particle counter vs. instrument supersaturation (considering depletion effects). Triangles denote simulations that correspond to "zero CCN" conditions (defined as CCN concentration below 500 cm^{-3}).

Figure 7: $\frac{s}{s_o}$ vs $\frac{D_p}{D_{po}}$ for (a) all the simulations presented in Figure 3, and, (b) the experiments presented in Figure 6a. Dashed lines correspond to ±10% deviation from the diagonal.

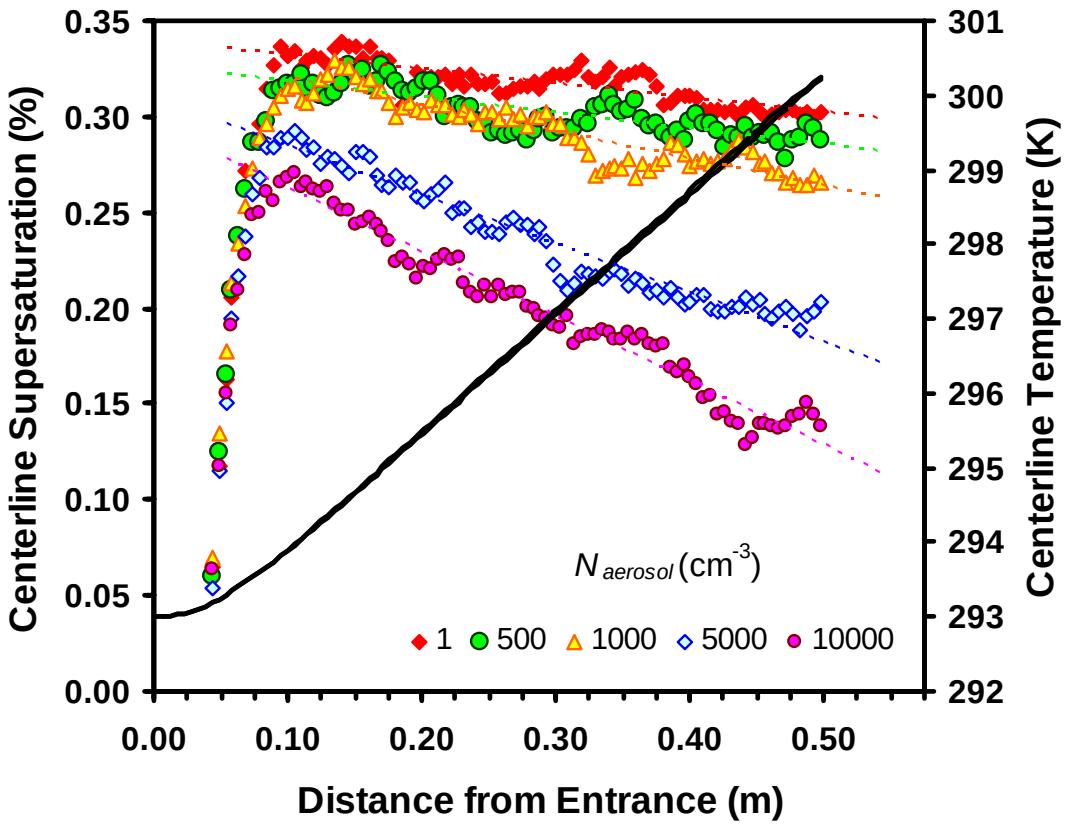
Centerline Supersaturation (%)
Centerline Temperature (K)
Distance from Entrance (m)
0.00
0.05
0.10
0.15
0.20
0.25
0.30
0.35
292
293
294
295
296
297
298
299
300
301
0.00
0.10
0.20
0.30
0.40
0.50
N aerosol (cm-3)
1
500
1000
5000
10000

Figure 1

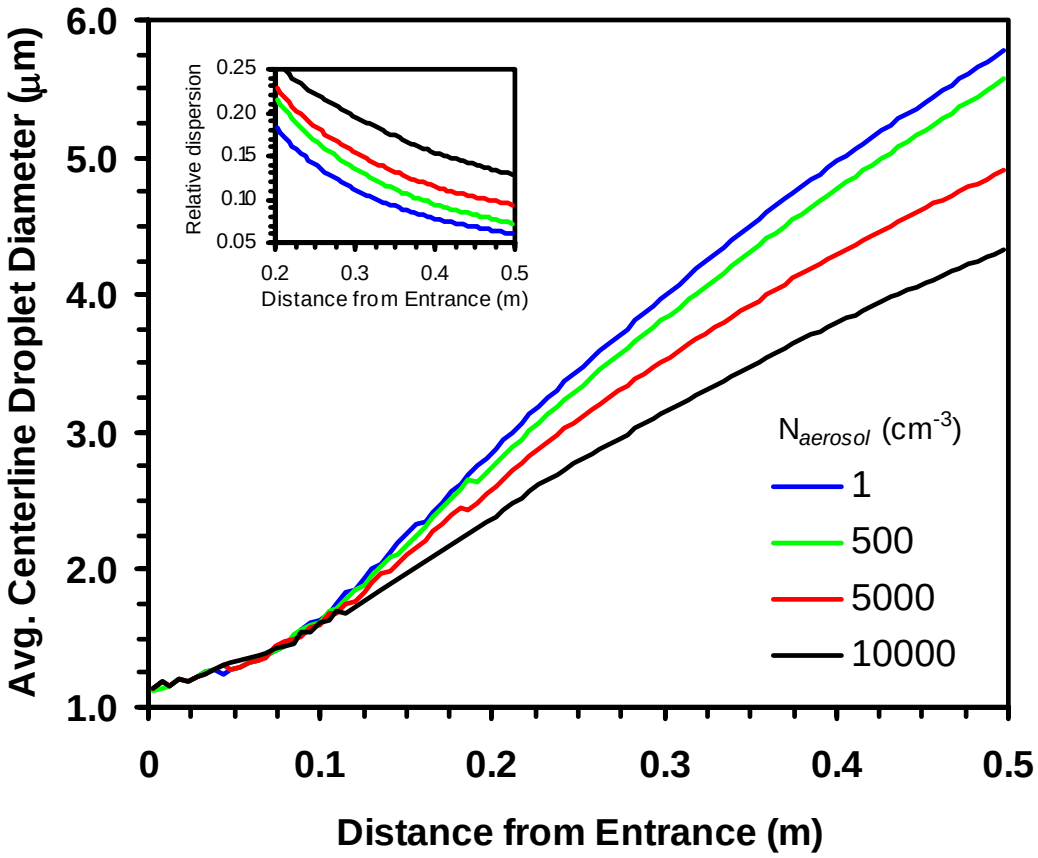
Avg. Centerline Droplet Diameter (μm)
6.0
5.0
4.0
3.0
2.0
1.0
0
0.1
0.2
0.3
0.4
0.5
Distance from Entrance (m)
Relative dispersion
0.25
0.20
0.15
0.10
0.05
0.2
0.3
0.4
0.5
Distance from Entrance (m)
N_aerosol (cm^-3)
1
500
5000
10000

Figure 2

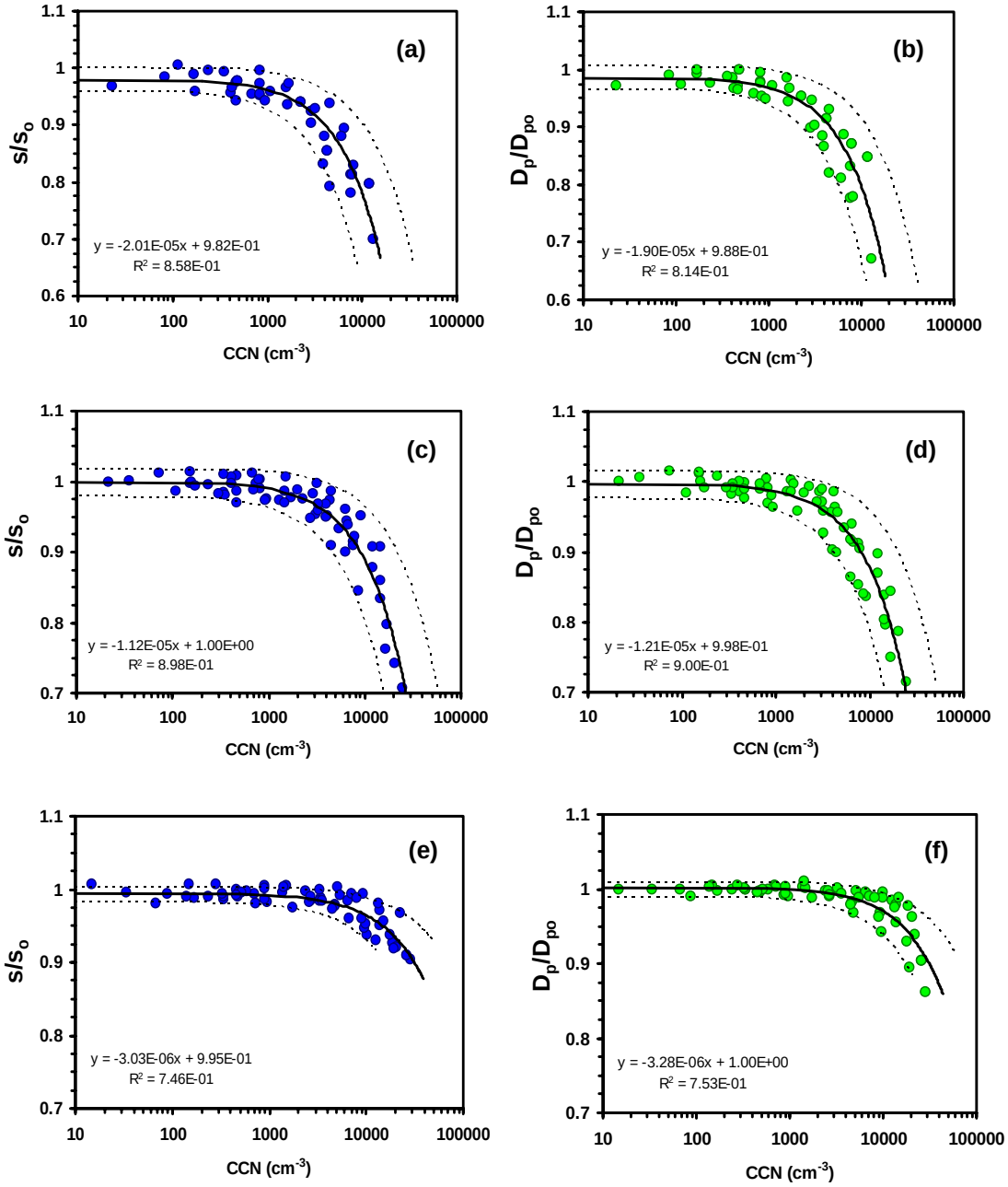
(a)
s/s$_o$
y = -2.01E-05x + 9.82E-01
R^2 = 8.58E-01
CCN (cm^{-3})
(b)
D$_p$/D$_{po}$
y = -1.90E-05x + 9.88E-01
R^2 = 8.14E-01
CCN (cm^{-3})
(c)
s/s$_o$
y = -1.12E-05x + 1.00E+00
R^2 = 8.98E-01
CCN (cm^{-3})
(d)
D$_p$/D$_{po}$
y = -1.21E-05x + 9.98E-01
R^2 = 9.00E-01
CCN (cm^{-3})
(e)
s/s$_o$
y = -3.03E-06x + 9.95E-01
R^2 = 7.46E-01
CCN (cm^{-3})
(f)
D$_p$/D$_{po}$
y = -3.28E-06x + 1.00E+00
R^2 = 7.53E-01
CCN (cm^{-3})

Figure 3

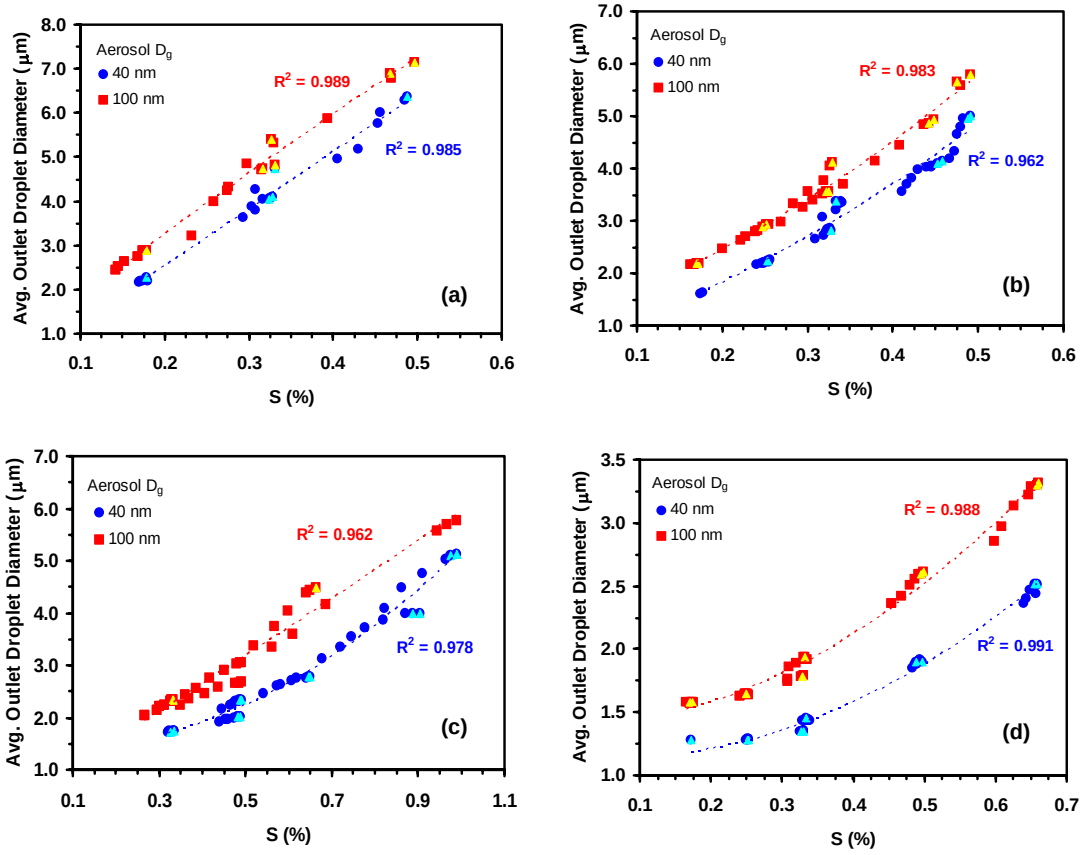
Aerosol D_g
40 nm
100 nm
R^2 = 0.989
R^2 = 0.985
(a)
Avg. Outlet Droplet Diameter (μm)
S (%)
R^2 = 0.983
R^2 = 0.962
(b)
R^2 = 0.962
R^2 = 0.978
(c)
R^2 = 0.988
R^2 = 0.991
(d)

Figure 4

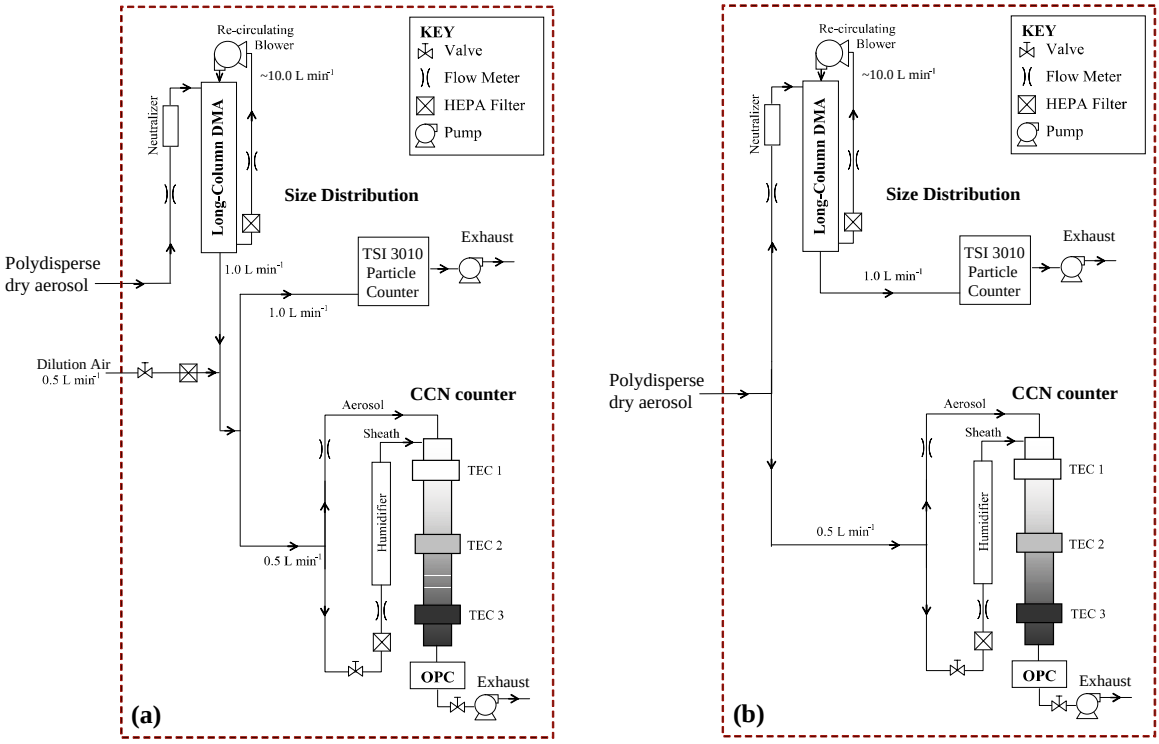
KEY
Valve
Flow Meter
HEPA Filter
Pump
Re-circulating Blower
~10.0 L min-1
Neutralizer
Long-Column DMA
Size Distribution
Polydisperse dry aerosol
1.0 L min-1
TSI 3010 Particle Counter
Exhaust
1.0 L min-1
Dilution Air
0.5 L min-1
CCN counter
Aerosol
Sheath
Humidifier
TEC 1
TEC 2
TEC 3
0.5 L min-1
OPC
Exhaust
(a)
(b)

Figure 5

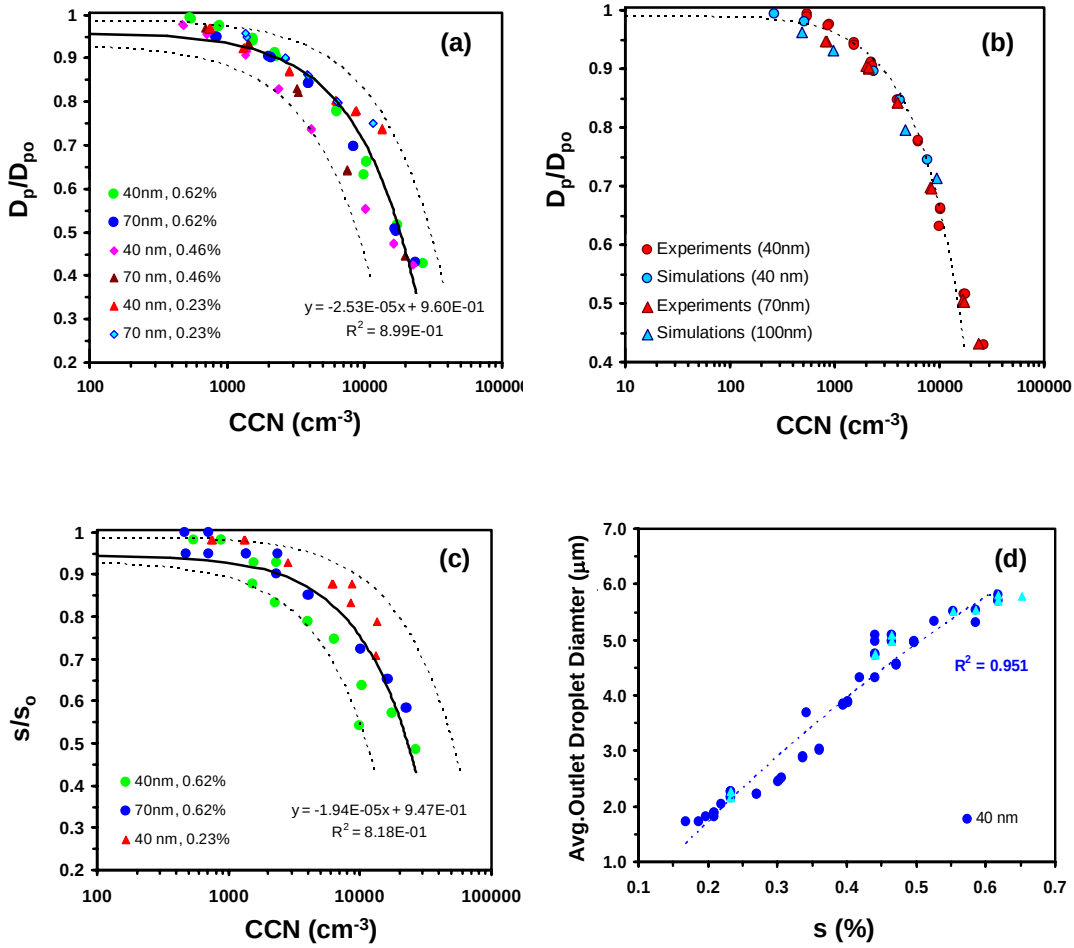
(a)
D_p/D_{po}
40nm, 0.62%
70nm, 0.62%
40 nm, 0.46%
70 nm, 0.46%
40 nm, 0.23%
70 nm, 0.23%
y = -2.53E-05x + 9.60E-01
R^2 = 8.99E-01
CCN (cm^{-3})
(b)
D_p/D_{po}
Experiments (40nm)
Simulations (40 nm)
Experiments (70nm)
Simulations (100nm)
CCN (cm^{-3})
(c)
s/s_o
40nm, 0.62%
70nm, 0.62%
40 nm, 0.23%
y = -1.94E-05x + 9.47E-01
R^2 = 8.18E-01
CCN (cm^{-3})
(d)
Avg.Outlet Droplet Diamter (µm)
R^2 = 0.951
40 nm
s (%)

Figure 6

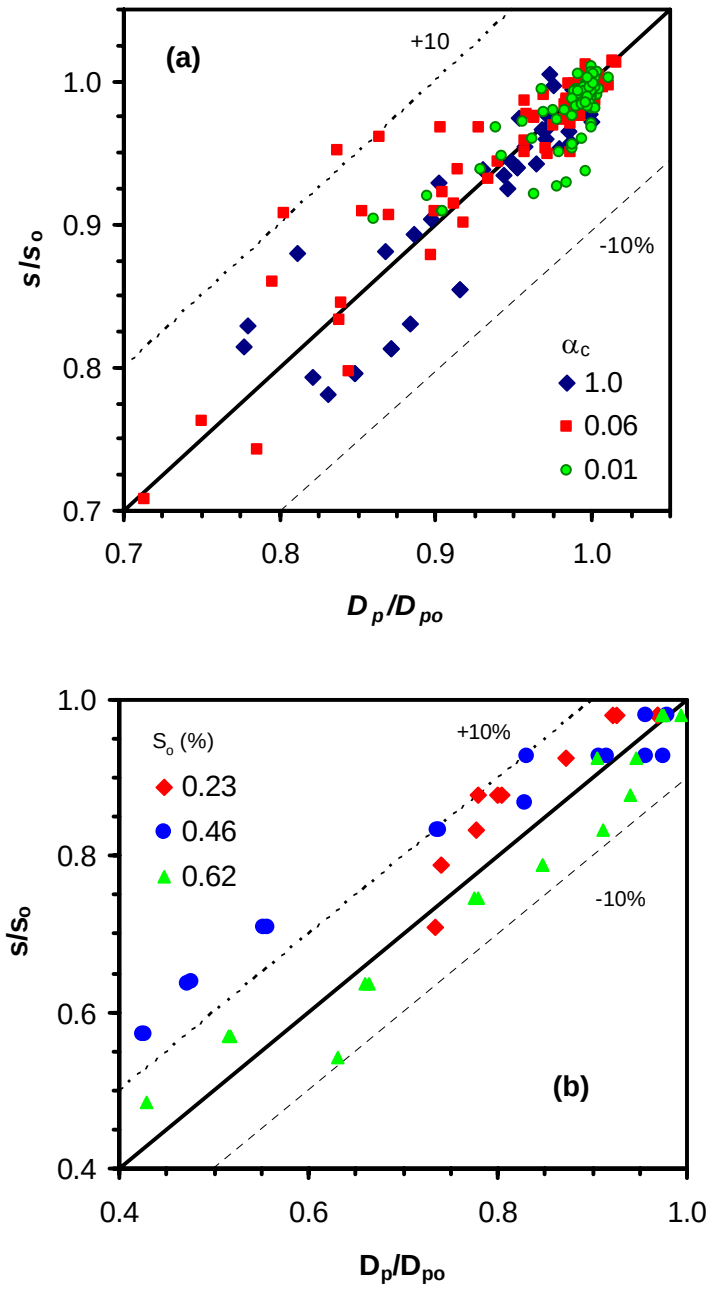

Figure 7